U.S. Department of Energy Reference Model Program RM1: Experimental Results

Craig Hill[1]
Vincent S. Neary[2]
Budi Gunawan[2]
Michele Guala[1]
Fotis Sotiropoulos[1]

[1]St. Anthony Falls Laboratory, College of Science & Engineering, University of Minnesota
[2]Water Power Technologies, Sandia National Laboratories

December 2, 2014

Prepared by:
St. Anthony Falls Laboratory
College of Science & Engineering
University of Minnesota
Minneapolis, MN

Prepared for:
Wind and Water Power Technologies Program
Office of Energy Efficiency and Renewable Energy
U.S. Department of Energy
Washington, D.C.

Contents

I. Introduction 3
II. Experimental Setup and Data Collection 3
III. Data Processing 8
IV. Results 11
V. Summary 18
VI. Acknowledgment 19
VII. References 19
VII. Appendix A: Tabulated summary of performance testing for RM1. 20
VIII. Appendix B: Inflow characteristics for $3d_T$ upstream of RM1. 21
IX. Appendix C: Inflow characteristics for $5d_T$ upstream of RM1. 22

I. Introduction

The Reference Model Project (RMP), sponsored by the U.S. Department of Energy's (DOE) Wind and Water Power Technologies Program within the Office of Energy Efficiency & Renewable Energy (EERE), aims at expediting industry growth and efficiency by providing non-proprietary Reference Models (RM) of MHK technology designs as study objects for open-source research and development (Neary et al. 2014a,b). As part of this program, MHK turbine models were tested in a large open channel facility at the University of Minnesota's St. Anthony Falls Laboratory (UMN-SAFL). Reference Model 1 (RM2) is a 1:40 geometric scale dual-rotor axial flow horizontal axis device with counter-rotating rotors, each with a rotor diameter d_T = 0.5m. Precise blade angular position and torque measurements were synchronized with three acoustic Doppler velocimeters (ADVs) aligned with each rotor and the midpoint for RM1. Flow conditions for each case were controlled such that depth, h = 1m, and volumetric flow rate, Q_w = 2.425m^{3}s^{-1}, resulting in a hub height velocity of approximately U_{hub} = 1.05ms^{-1} and blade chord length Reynolds numbers of $Re_c \approx 3.0\text{x}10^5$. Vertical velocity profiles collected in the wake of each device from 1 to 10 rotor diameters are used to estimate the velocity recovery and turbulent characteristics in the wake, as well as the interaction of the counter-rotating rotor wakes. The development of this high resolution laboratory investigation provides a robust dataset that enables assessing turbulence performance models and their ability to accurately predict device performance metrics, including computational fluid dynamics (CFD) models that can be used to predict turbulent inflow environments, reproduce wake velocity deficit, recovery and higher order turbulent statistics, as well as device performance metrics.

II. Experimental Setup and Data Collection

Experiments for the RM1 were completed in the Main Channel facility at the University of Minnesota's St. Anthony Falls Laboratory (SAFL). This channel is a 2.75*m* wide by 1.8*m* deep x 85*m* long channel supplied with continuous and untreated Mississippi River water. An intake gate controls the discharge level within the flume while a mechanical tailgate weir controls the flow depth and monitors flow rate. Water passes through two rows of vertically oriented baffles to break up any large scale turbulent structures before entering the test section of the channel. The RM1 model was located approximately 40m downstream of the baffles. RM1 is a 1:40 geometric scale dual-rotor axial flow horizontal axis device with counter-rotating rotors, each with a rotor diameter d_T = 0.5m. Various geometric and experimental hydraulic characteristics are detailed in Tables 1 and 2. The blade profile used for the SAFL RM1 turbine designs (NACA 4415) was modified from the original RM1 design blade profile (NACA 63(4)-24). This was done because of the lower Reynolds number flows used for the SAFL open channel experiments and the availability of low Reynolds number lift (C_L) and drag (C_D) coefficient data for the NACA 4415 profile. Schematics and photos of the experimental setup are illustrated in Figures 1 through 3. The SAFL Main Channel is equipped with a Data Acquisition (DAQ) Carriage that is capable of three-axis automated motion. This carriage was utilized during data collection to position various sensors to monitor the hydraulic environment around the RM1. Additional details of the experimental plan are discussed in Neary et al. (2012).

Continuous discharge measurements were recorded at rates typically set to 1 Hz. Discharge was measured using a Massa M5000 ultrasonic range sensor to measure water surface elevation upstream of the tailgate weir. Discharge values are then calculated using a calibrated sharp-crested weir equation,

$$Q_{LPS} = 1838LH^{3/2}$$

where Q_{LPS} is the volumetric discharge rate in liters per second, L is the weir width (L = 2.75m) and H is the measured depth passing over the weir (H = water surface elevation – weir elevation).

Velocity measurements were collected using three Nortek Vectrino acoustic Doppler velocimeters (ADVs). During performance measurements, the ADVs were positioned at hub height 3 rotor diameters ($3d_T$) upstream of the RM1 rotor location and sampled at 200Hz for 10 minutes for each rotor angular velocity. All three ADVs were synchronized with the turbine torque and angular position measurements. Vertical velocity profiles were collected at $1d_T$, $3d_T$ and $5d_T$ upstream of the RM2 location. Vertical point spacing was 5cm and measurements were collected at 200Hz for 3 minutes. A horizontal profile at hub height was collected at $1d_T$, $3d_T$ and $5d_T$ upstream and spanned the channel width. Wake vertical velocity profiles were collected downstream of the turbine from $1d_T$ to $10d_T$ with $1d_T$ streamwise spacing. One ADV was aligned with the axis of rotation for each rotor, and the third ADV was positioned at the mid-plane between the rotors centered on the vertical cylindrical support tower for RM1. Vertical point spacing was 2.5cm for all wake profiles, and measurements were collected for 5 minutes at each point at 200Hz. A horizontal plane was collected from $1d_T$ to $10d_T$ with $1d_T$ streamwise spacing. Cross-stream ADV point location varied, but provided enough spatial resolution to resolve key characteristics of the turbine wake. Prior to velocity measurements, the SAFL Main Channel was ponded with water and a towing test was performed to determine any rotation of the ADV measurement volume. All measurements had the resulting rotation matrix applied to the data before calculating flow statistics. Additionally, velocity timeseries measurements were filtered to remove any erroneous samples (Gunawan et al. 2011).

Torque measurements were collected from each rotor. Each rotor had an Interface Force 20Nm MRT miniature reaction torque sensor mounted inside the hub, thereby minimizing the torque losses in the system prior to measuring torque. Voltages from the torque transducer were transmitted to the data acquisition computer via a Rotary Systems SR003 series slip ring, through an Interface Force SGA signal conditioner to convert the millivolt signal to a 0-5V range, and then acquired at the analog to digital data acquisition board. A chain drive was used to connect the shaft of each rotor to the shaft of the system speed control. A Pacific Scientific stepper motor (model K42HRFM-LEK-M2-00) controlled by a Parker Zeta 6108 indexer drive provided accurate and precise control of rotor angular velocity. Angular position was measured using a single Automation Direct rotary encoder (model TRD-SH1000-VD) mounted to the motor shaft and referenced to the counter-rotating RM1 rotor blade position. All torque and angular position measurements were synchronized with the velocity measurements.

RM1 (Tidal Turbine) - 1:40 scale	
Parameter	**SAFL Turbine Geometries**
Blade Profile	NACA 4415
Max Chord Length	0.0645 m
Tip Chord Length	0.0312 m
Rotor Diameter (d_T)	0.5 m
Hub Height (h_{hub})	0.5 m ($1.0d_T$)
Hub Diameter (d_{hub})	0.087 m ($0.174d_T$)
Hub Length (L_{hub})	0.080 m
Nacelle Length (L_N)	0.380 m
Nacelle Diameter (d_N)	0.095 m ($0.19d_T$)
Cross Arm attachment position	L_N x 53.4%
Cross Arm Diameter	0.0762 m
Vertical Tower diameter	0.0889 m
Rotor Spacing (S)	0.7 m ($1.4d_T$)
Submergence	0.5 m ($1.0d_T$)
Solidity	13.7%
Flow Depth (h)	1.0 m ($2.0d_T$)
Volumetric Flow Rate (Q_w)	2.425 m^3s^{-1}
Blockage ($= A_T/A$)	14.3%
Tip-Speed Ratios	1 to 9
Froude Number	0.28 ($U_\infty \approx 0.88$ ms^{-1})
Reynolds Number ($R_c = \lambda \cdot U_{hub} \cdot L_c / \nu$)	$\approx 3.0 \times 10^5$

Table 1: Characteristics of the 1:40 scale RM1 SAFL model turbine.

r/R (-)	Radius (mm)	Pre-Twist (deg)	Chord (mm)	% Thick (t/c)	Thickness (mm)
0.21	53.3	13.16	30.0	100.0	30.0
0.24	60.0	13.16	30.0	100.0	30.0
0.27	66.7	13.16	34.2	84.9	29.0
0.29	73.3	13.16	46.8	51.8	24.2
0.32	80.0	13.16	57.2	31.1	17.8
0.35	86.7	13.16	62.6	19.4	12.1
0.37	93.3	13.16	64.5	15.0	9.7
0.40	100.0	11.28	64.4	15.0	9.7
0.43	106.7	10.24	63.2	15.0	9.5
0.45	113.3	9.43	61.5	15.0	9.2
0.48	120.0	8.76	59.5	15.0	8.9
0.51	126.7	8.17	57.4	15.0	8.6
0.53	133.3	7.64	55.3	15.0	8.3
0.56	140.0	7.16	53.2	15.0	8.0
0.59	146.7	6.70	51.1	15.0	7.7
0.61	153.3	6.27	49.2	15.0	7.4
0.64	160.0	5.86	47.3	15.0	7.1
0.67	166.7	5.46	45.6	15.0	6.8
0.69	173.3	5.07	44.0	15.0	6.6
0.72	180.0	4.69	42.4	15.0	6.4
0.75	186.7	4.31	40.9	15.0	6.1
0.77	193.3	3.93	39.5	15.0	5.9
0.80	200.0	3.55	38.2	15.0	5.7
0.83	206.7	3.17	37.0	15.0	5.5
0.85	213.3	2.78	35.8	15.0	5.4
0.88	220.0	2.38	34.6	15.0	5.2
0.91	226.7	1.98	33.5	15.0	5.0
0.93	233.3	1.57	32.3	15.0	4.9
0.96	240.0	1.14	31.2	15.0	4.7
1.00	250.0	0.70	30.0	15.0	4.5

Table 2: Characteristics of the 1:40 scale RM1 SAFL model turbine blades (NACA 4415). The blade profile was changed from the original RM1 design (NACA 63(4)-24) to the NACA 4415 for the SAFL RM1 tests because the NACA 4415 design has Reynolds number experimental lift (C_L) and drag (C_D) coefficient data available.

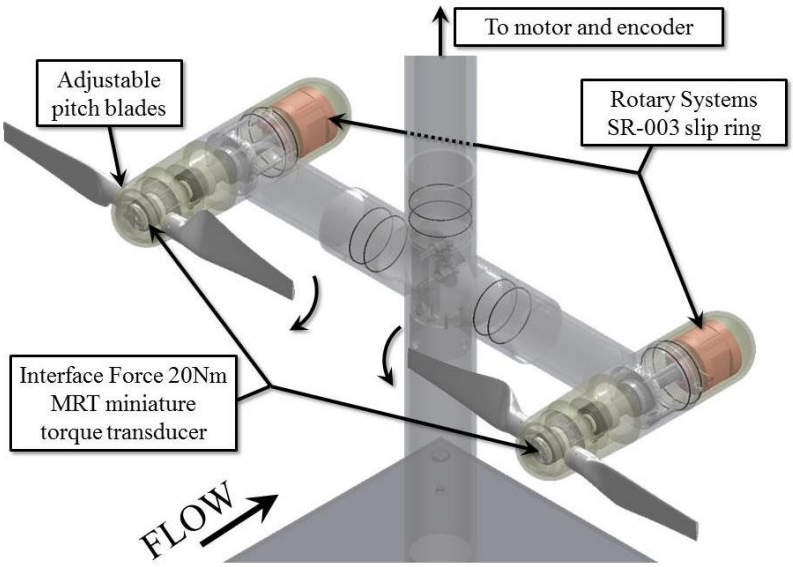

Figure 1: CAD rendering and instrumentation schematic of the RM1 model.

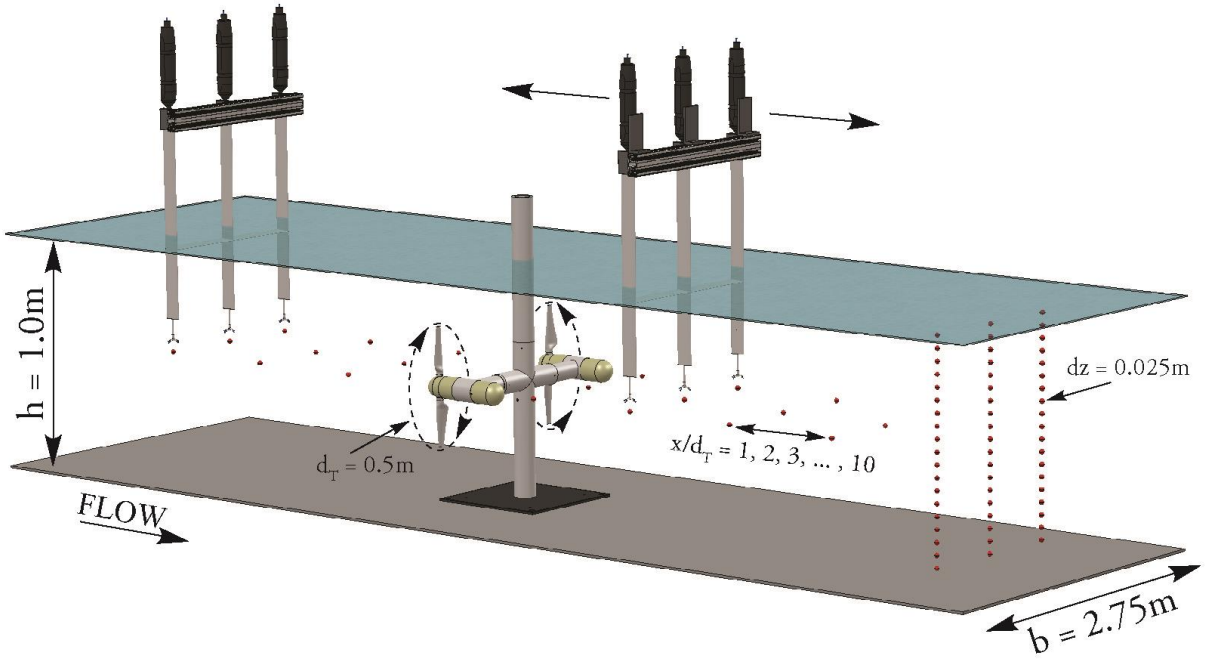

Figure 2: Schematic of the RM1 experimental setup and ADV collection locations in the SAFL Main Channel facility. Flow is from left to right.

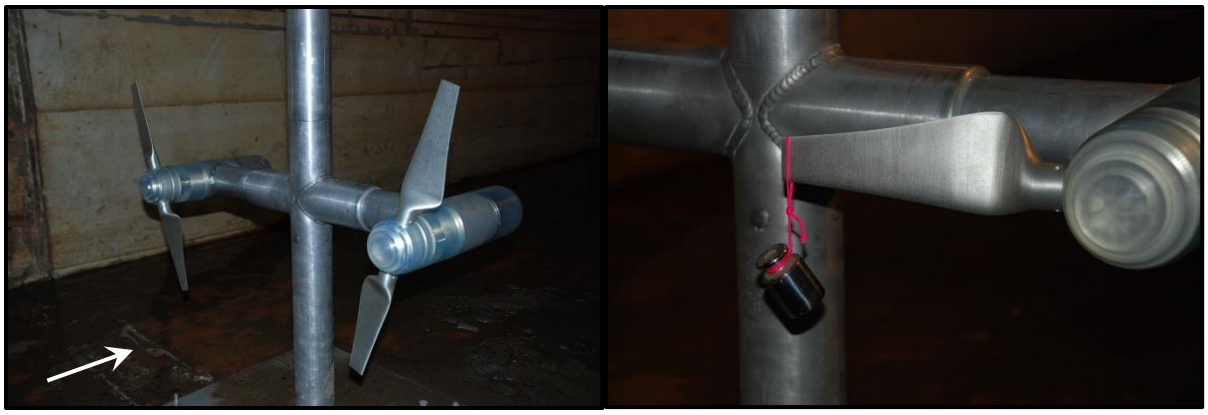

Figure 3: Photos of the RM1 dual-rotor model in the SAFL Main Channel (left) and during torque sensor calibration (right) performed by applying known forces to the rotor and torque sensor.

III. Data Processing

The following parameters were calculated during the processing of the velocity and turbine performance data collected during the RM1 experiments at SAFL.

a. Mean and fluctuating velocity fields

The 200Hz velocity data output from the three Nortek Vectrino velocimeters were filtered to remove any erroneous data (see Goring and Nikora 2002; Gunawan et al. 2011). Through Reynolds decomposition, the velocity timeseries can be decomposed into the mean and fluctuation components,

$$U_i = \overline{U} + u'$$

The so calculated fluctuating velocity components are then used to calculate a number of flow statistics, which are described below.

b. Turbulence Intensity

The turbulence intensities are dimensionless parameters that describe the level of turbulence within the flow along each spatial direction, and are defined as the root-mean squared of the fluctuating velocity component divided by the mean velocity magnitude, $\overline{U}_M = \sqrt{\overline{U}^2 + \overline{V}^2 + \overline{W}^2}$.

$$I_U = \frac{\sqrt{\overline{u'^2}}}{\overline{U}_M} \; ; \qquad I_V = \frac{\sqrt{\overline{v'^2}}}{\overline{U}_M} \; ; \qquad I_W = \frac{\sqrt{\overline{w'^2}}}{\overline{U}_M}$$

c. Reynolds Stresses

The Reynolds stress tensor is defined as follows:

$$\tau_{ij} = \overline{\overline{u'_i u'_j}}$$

when $i = j$, the results are the normal stresses ($\overline{u'u'}$, $\overline{v'v'}$, and $\overline{w'w'}$), also known as the velocity variance, and when $i \neq j$, the results are the shear stresses ($\overline{u'v'}$, $\overline{u'w'}$, and $\overline{v'w'}$).

d. Turbulence Kinetic Energy

The turbulence kinetic energy (TKE), *k*, is defined as follows:

$$k = \frac{1}{2}\left(\overline{u'^2} + \overline{v'^2} + \overline{w'^2}\right)$$

e. Velocity Deficit

The streamwise velocity deficit is a common metric used to report the wake velocity recovery downstream of a turbine, and is defined as follows:

$$\overline{U}_{def} = \frac{|\overline{U}_\infty - \overline{U}_x|}{\overline{U}_\infty}$$

where $\overline{U}_\infty$ is the upstream approach velocity at hub height, or rotor height center in the case of RM1, and $\overline{U}_x$ is the hub height velocity at position *x* downstream of the turbine. Here, $\overline{U}_\infty$ is measured at x/d_T = -5.

f. Turbine Performance

Using the synchronous velocity, torque and rotor position measurements, various turbine parameters could be calculated. The rotor position was used to calculate the turbine angular velocity, ω. Turbine power, P_T, was calculated using the measured torque and angular velocity using,

$$P_T = \tau\omega$$

where τ is the measured torque and ω is the calculated angular velocity that was applied via the stepper motor and measured using the positional encoder integrated with the drive system. The available power within the approaching flow was calculated using the synchronous velocity measurements upstream of the RM1 location using,

$$P_A = \frac{1}{2}\rho A_T U^3$$

where P_A is the calculated available power, ρ is the density of water (≈ 1 *kg/m*^{3}) dependent on water temperature (typically between 18.0°C and 20.5°C during the RM1 tests), A_T is the flow cross sectional area covered by the device ($A_T = \pi(d_T/2)^2$), and $\overline{U}$ is the approach flow mean velocity from the measured data using the 3 ADVs at hub height $3d_T$ upstream of the RM1. Both time-averaged turbine power ($\overline{P_T} = f(\bar{\tau})$) and available power ($\overline{P_A} = f(\overline{U})$) as well as instantaneous turbine power ($P_{T_i} = f(\tau_i)$) and available power ($P_{A_i} = f(U_i)$) were calculated. With these power calculations, the coefficient of performance, C_P, is calculated by applying the above defined values to the equation,

$$C_P = \frac{P_T}{P_A}$$

This parameter describes the fraction of power extracted from the approaching flow by the turbine. An additional dimensionless parameter used to describe the turbine performance characteristics is the tip-speed ratio, λ, defined as the ratio of the rotor tip speed to the speed of the approaching flow,

$$\lambda = \frac{\omega R}{\bar{U}}$$

Detailed performance testing characteristics for each scenario are presented in the tables in Appendix A.

g. Uncertainty Analysis

In experimental measurements, both systematic and random measurement error exists (Coleman and Steele, 2009). Systematic error in the torque sensors was determined during torque sensor calibration (see Figure 3) by applying known torque values and comparing measured against expected values. The results of the calibration tests are summarized in Table 3 and represent the systematic (constant) error associated with the torque sensors during RM1 experiments. This systematic error was removed prior to calculating and reporting of the additional experimental measurement uncertainty. Uncertainty values for the ADVs and optical encoder were used from manufacturer's reported values and incorporated into the error propagation from measurements into the calculations of turbine performance, C_p. Additionally, extended datasets were collected to assess the uncertainty in the mean values of each instrument. Results showed that the uncertainty in the torque, τ, was $U_\tau / \tau = 1.92\%$. Uncertainty in the angular velocity, ω, was $U_\omega / \omega = 2.5\%$. Uncertainty in the velocity measurements, U, was $U_U / U = 0.78\%$. Methods outlined by Coleman and Steele (2009) were used to calculated the combined uncertainty from the measured variables used in calculating $C_p = f(\tau, \omega, U^3)$. The uncertainty in calculated C_p values is given by;

$$\left(\frac{U_{C_P}}{C_P}\right)^2 = \left(\frac{U_\tau}{\tau}\right)^2 + \left(\frac{U_\omega}{\omega}\right)^2 + (-3)^2\left(\frac{U_U}{U}\right)^2$$

Using the uncertainty values reported above, the uncertainty in calculated C_p values is approximately $U_{CP} \approx 3.9\%$.

Right Rotor				
Expected Torque (Nm)	**Measured Torque (Nm)**	**% Error**	**Scaled Torque (Nm)**	**New % Error**
-2.184	-2.172	-0.56%	-2.182	-0.08%
-1.093	-1.078	-1.37%	-1.083	-0.89%
-0.545	-0.534	-2.02%	-0.537	-1.55%
0.545	0.546	0.14%	0.549	0.62%
1.093	1.092	-0.09%	1.097	0.39%
2.184	2.179	-0.22%	2.190	0.27%
	Average Error	**-0.69%**		**-0.21%**
	Scaling Factor	**1.005**		

Left Rotor				
Expected Torque (Nm)	**Measured Torque (Nm)**	**% Error**	**Scaled Torque (Nm)**	**New % Error**
-2.184	-2.107	-3.54%	-2.188	0.17%
-1.093	-1.050	-3.96%	-1.090	-0.27%
-0.545	-0.524	-3.83%	-0.545	-0.14%
0.545	0.524	-3.94%	0.544	-0.24%
1.093	1.052	-3.76%	1.093	-0.06%
2.184	2.102	-3.76%	2.183	-0.07%
	Average Error	**-3.80%**		**-0.10%**
	Scaling Factor	**1.038**		

Table 3: Torque sensor calibration summary for RM1.

IV. Results

a. Inflow Characteristics

Inflow velocity profiles were collected at 3 rotor diameters ($3d_T$ = 1.5m) and 5 rotor diameters ($5d_T$ = 2.5m) upstream of the RM1 rotor locations. The 3 ADV mount described in the Experimental Setup section was use to collect synchronous ADV measurements at these two vertical velocity profile locations. Average hub height streamwise velocity, U_{hub} = 1.05m/s. Turbulence intensity in the region of the RM1 rotors was approximately 5%. Summary statistics for the mean velocity ($\overline{U}$, $\overline{V}$, and $\overline{W}$), fluctuating velocities ($\sqrt{\overline{u'^2}}$, $\sqrt{\overline{v'^2}}$, and $\sqrt{\overline{w'^2}}$), and turbulence intensity (I_U, I_V, and I_W) are presented in Appendix B ($3d_T$ upstream) and C ($5d_T$ upstream). An additional vertical velocity profile was collected at $1d_T$ upstream of the RM1 turbine; however, the proximity of the turbine effected the flow at this location so is not representative of the undisturbed flow environment in the channel.

b. Shear Velocity

The shear velocity, u_*, in open channel flow is an important parameter in characterizing the near-wall stresses imposed by the flow on the channel boundaries. This parameter can be estimated using velocity profiles and the logarithmic law of the wall equation,

$$\frac{\overline{U}}{u_*} = \frac{1}{\kappa}\ln\left(\frac{z}{z_0}\right)$$

where $\overline{U}$ is the mean velocity at z, the distance from the wall, κ is the von Karman constant (κ = 0.41), and z_0 is the hydrodynamic roughness length. The velocity profiles measured upstream of the RM1 are plotted in Figure 4. Using this method, the friction velocity was found to be, u_* = 0.033m/s.

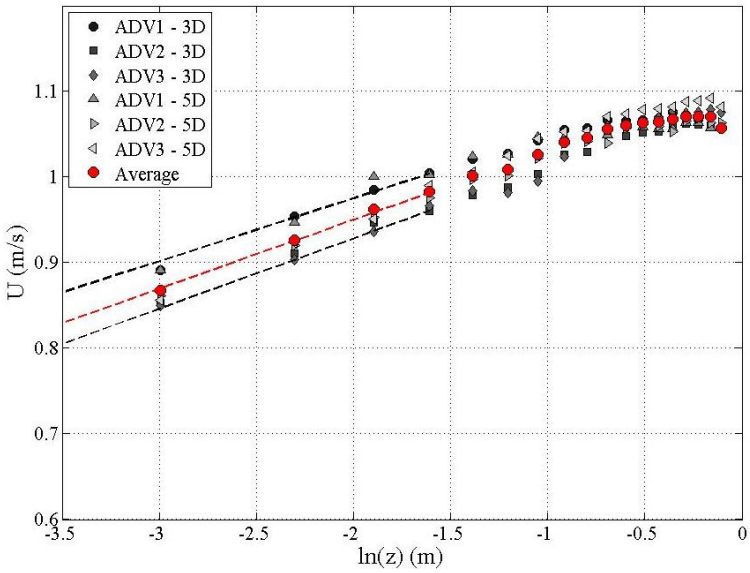

Figure 4: Plot of inflow velocity, $\overline{U}$, against the natural log of the elevation, *ln(z)*. Lower 20% of the inflow profiles used to estimate friction velocity, u_*, and hydrodynamic roughness length, z_0, using the logarithmic law of the wall equation. Red points indicate average values from the six inflow profiles collected. Red dashed line represents linear trendline against the averaged points. Black dashed lines indicated maximum and minimum linear trendlines against the data for estimating u_* and z_0.

c. *Turbine Performance*

Performance curves for both the left and right rotors are shown in Figure 5. These plots show the coefficient of power against tip-speed ratio. Optimal performance occurred at approximately $\lambda = 5.1$ with a corresponding $C_P = 0.48$ for the right rotor and $C_P = 0.43$ for the left rotor. For comparison, Lust et al. (2013) observed optimal performance at approximately $\lambda = 6.5$ with a corresponding $C_P = 0.41$ for a single scaled model RM1 rotor in a large towing tank facility at the United States Naval Academy. The turbine model for the Naval Academy test consisted of a 0.8 m diameter rotor with a NACA 63-618 blade cross section. The blades are twisted from 13° at the root to 2° at the tip and tapered from a maximum chord length of 0.07m to a minimum of 0.025 cm. Detailed performance testing characteristics for each scenario are presented in the tables in Appendix A. The two rotors performed differently, although both had relatively high performance (i.e. greater than $C_P = 0.4$). The complexity of flow in the SAFL open channel facility and slight asymmetry in the approach flow may have been a factor in this observed difference. In addition to the measurement uncertainty reported in Figure 5, possible differences could result from asymmetric flow. Because turbine performance is a function of velocity cubed, $C_p = f(U^3)$, a difference of 0.03-0.05ms^{-1} (≈ 3-5% in the RM1 experiments case) from one side of the channel to the other could result in C_p values varying by approximately 9-15%. The resulting performance curves do show differences at optimal tip speed ratio, λ, of approximately 10%. During performance tests, ADVs were positioned upstream at $3d_T$ and aligned with the rotor center. These velocity values were used in calculating instantaneous C_p values; however, additional asymmetry in the approach flow that may have existed to the left or right of the ADV, yet still within the turbine energy extraction plane region, may have propagated and added to the difference in calculated C_p values.

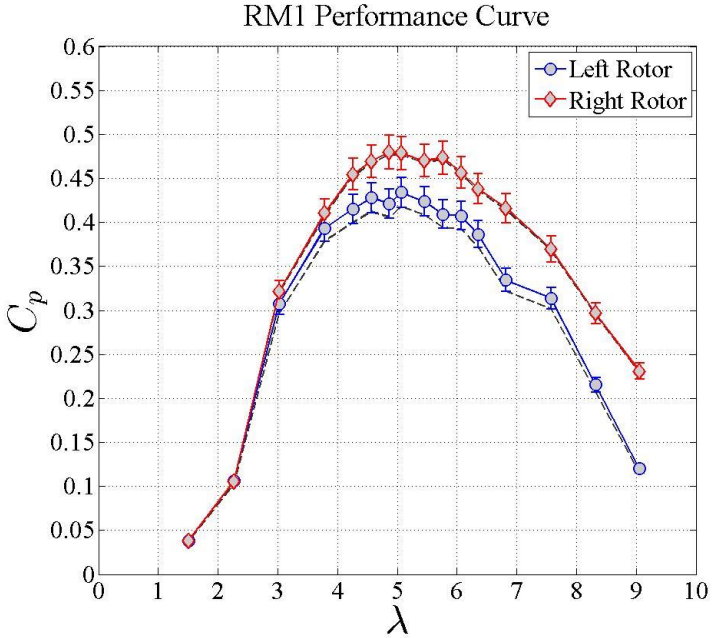

Figure 5: Calculated C_P vs. λ (coefficient of power vs. tip-speed ratio) for the left (blue) and right (red) RM1 rotors. Dashed gray lines represent the C_P curves before scaling the torque values based on torque sensor calibration. Vertical error bars represent mean C_P value measurement uncertainty. After scaling corrections, maximum C_P occurs near $\lambda \approx 5.1$ (right rotor $C_P = 0.48$; left rotor $C_P = 0.43$). Experimental conditions for the performance testing were $Q_w \approx 2.425$ m^{3}s^{-1}, $h = 1.0$m, and $U_{hub} \approx 1.05$ ms^{-1}. NOTE: Results have not been corrected for channel blockage; therefore, may be slightly reduced after blockage corrections have been applied.

d. Blade Pitch Alignment

Initial performance testing of the RM1 rotors revealed a C_P vs. λ curve as shown in Figure 5. It was hypothesized that the pitch of the blades on the left rotor were misaligned, thereby creating the lowered performance compared to the right rotor. To investigate this hypothesis, performance measurements at several pitch angles for the left rotor were measured to verify that the blades were at the optimal angle. After collecting performance measurements at a turbine rotational speed of ω = 3.4rps ($\lambda \approx 5.1$), it was found the optimal pitch angle was $\alpha = 0°$ for the initial performance tests completed (Figure 6). Therefore, other factors, not identified in this study, caused decreased performance of the left rotor. A full round of performance testing was repeated. These are the results shown in Figure 5.

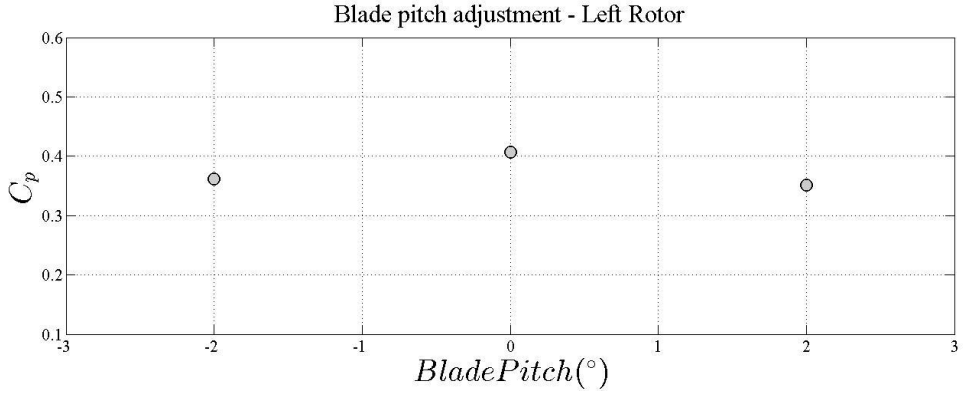

Figure 6: Blade pitch angle verification tests for the RM1 left rotor. Optimal performance was found to be at pitch angle of $\alpha = 0°$ ($C_p \approx 0.41$). Performance measurements were repeated with this angle and reported in Figure 5.

e. Turbine Wake Characteristics

Turbine wake velocity profiles were collected downstream of the RM1 rotor locations from $1d_T$ to $10d_T$ at $1d_T$ streamwise spacing. These data were collected along 3 vertically oriented (XZ) planes aligned with each rotor center and the mid-plane between the two rotors, as well as a horizontal (XY) plane aligned with the rotor hub height (Figure 7). Contour plots for the normalized mean streamwise velocity within the horizontal hub height plane are shown in Figure 8. Values have been normalized by the approaching flow velocity at the corresponding location upstream of the RM1 turbine. Additionally, the normalized values of turbulent kinetic energy in the horizontal plane are illustrated in Figure 9. Similar quantities are reported for each of the three vertical velocity planes collected upstream and downstream of the RM1 turbine in Figures 10 (normalized streamwise velocity) and 11 (normalized turbulent kinetic energy). In general, the largest velocity deficit occurs in the near wake region at the center between the two rotors, immediately downstream of the center cylindrical vertical and horizontal support arms. The relatively high blockage (14.3%) forces flow acceleration to the outside of each rotor, as well as above and below each rotor location, visible in figures 8 and 10. It should be noted that the results reported here have not yet been corrected for channel blockage. The wake of each RM1 rotor quickly joins with the disturbance created by the center tower and forms a horizontally expansive wake that propagates far downstream and remains approximately the width of the entire RM1 device while slowly diffusing and mixing with the surrounding flow. Elevated levels of turbulent kinetic energy are present in the downstream environment, particularly in the region aligned with the center support tower extending to approximately $2d_T$. Additionally, the tip vortices shed from the blades create elevated

regions of turbulent kinetic energy, evident in Figure 11 aligned with the top-tip elevation of each rotor. Between approximately $2d_T$ and $4d_T$, the TKE values begin to spread vertically and horizontally.

It is also common to report the velocity deficit downstream of a turbine as a way to estimate the velocity recovery in the wake of the device. The streamwise velocity deficit previously defined is plotted at the RM1 rotor hub height, along with streamwise root-mean squared (RMS) fluctuation values and streamwise turbulence intensity, in Figure 12. The RM1 rotors begin affecting inflow velocities up to approximately $2.5d_T$ to $3d_T$, at which point the flow decelerates by approximately 10% by the time it is one blade length upstream of the rotor energy extraction plane. The largest velocity deficit occurs in the wake of the center support tower (approximately 100%), which strong instabilities occurring here in the form of von Karman type vortices shed from the cylinder. Near wake ($\approx 1d_T$) velocity deficit in the wake of each rotor is approximately 30% and increases up to about $3d_T$ to $4d_T$, at which point it begins to gradually recover. The relatively large blockage by the two rotors and center cylinder support tower generate a large wake that propagates far downstream. Hub height velocity measurements were collected up to $24d_T$, at which point the velocity deficit had recovered to only about 5% in the wake of each rotor, while the center of the wake was still nearly 15% deficient. Neither turbulent fluctuations nor the streamwise turbulence intensity recovered to the undisturbed upstream equivalent values as far downstream as $24d_T$.

Wake characteristics from previous experiments using a single 3-bladed axial flow turbine with the same diameter, d_T = 0.5m, were reported by Chamorro et al. (2013) and wake recovery was discussed by Neary et al. (2013). The rotor for this turbine was located on the downstream side of the support tower (d_{tower} = 0.038m), whereas the RM1 dual-rotor turbine rotors were located on the upstream side of the horizontal cross arm supports. Results presented in Neary et al. (2013) show a similar behavior in the velocity deficit, with a peak velocity deficit occurring around $x/d_T = 3$. The near wake velocity deficit for the RM1 turbine is lower than the single rotor turbine, possibly due to the larger size, proximity, and downstream near-wake location of the horizontal cross arm support. The flow instability generated by this support structure could increase mixing, thereby increasing wake mixing and decreasing recovery distance. Far wake (greater than $x/d_T = 5$) velocity deficit is similar between the single rotor and dual-rotor turbines ($\approx$ 10%-20%). Similar behavior is also noticed in the RMS values, with peak intensity occurring around $x/d_T = 5$; however, single rotor turbine values are approximately twice that of the RM1 dual-rotor turbine. Turbulence intensity, I_U, values are similar for distances greater than $x/d_T = 5$, but lower in the near wake region closer than $x/d_T = 5$.

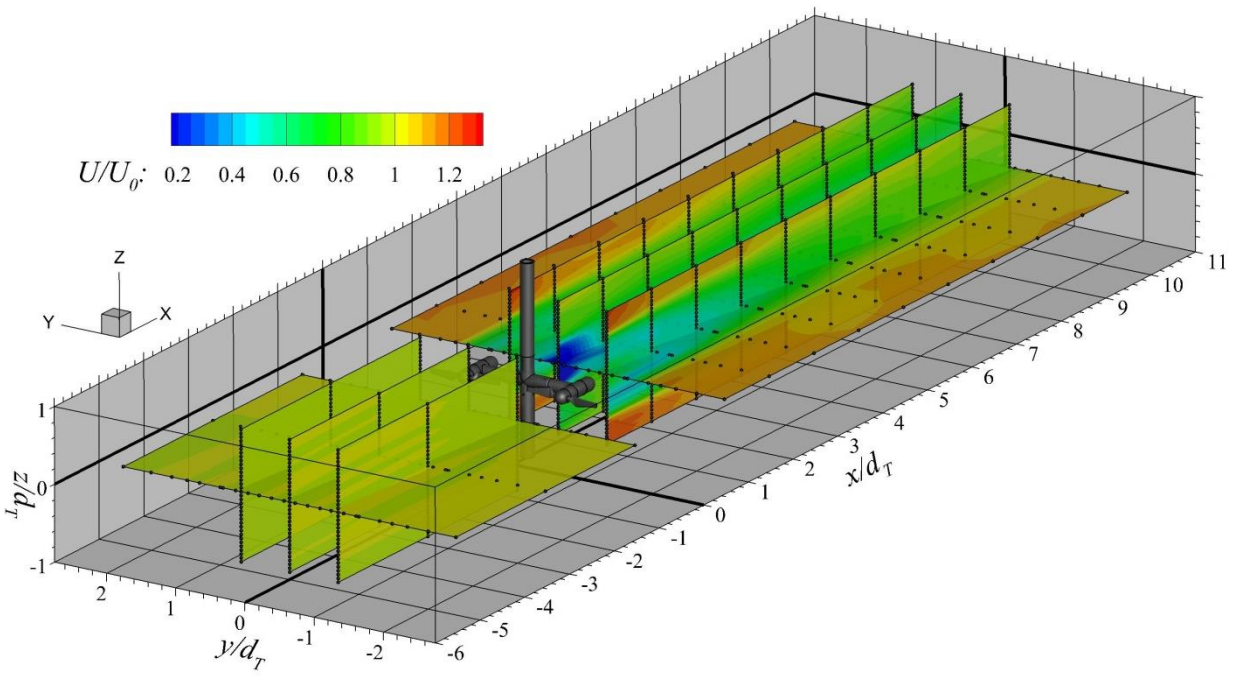

Figure 7: 3D view of the velocity data collected in the SAFL Main Channel upstream and downstream of the RM1 dual-rotor axial-flow turbine. Black circles represent ADV sampling locations used to produce contour plots of normalized streamwise velocity. RM1 model shown at $x/d_T = 0$ in gray. Flow is left to right. Axes have been normalized by RM1 rotor diameter, $d_T = 0.5$m. Measurements collected at $\lambda \approx 5.1$ ($\omega = 3.4$ rps).

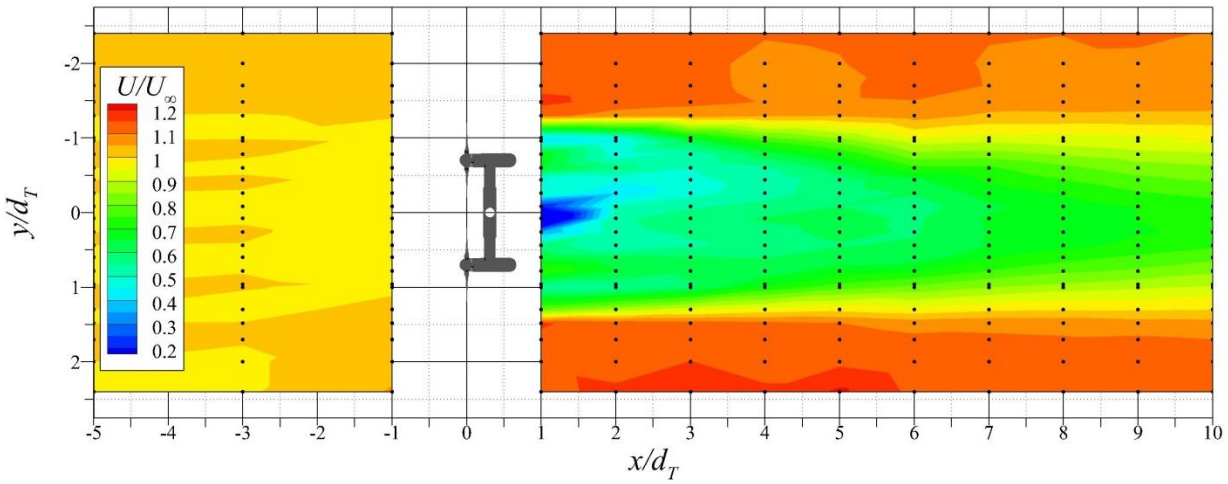

Figure 8: Normalized streamwise velocity horizontal plane (XY) contours downstream of RM1 in the SAFL Main Channel. Vertical axis, y/d_T, shows full SAFL Main Channel width ($b = 2.75$m). Black dots indicate actual ADV measurement locations. Measurements collected at $\lambda \approx 5.1$ ($\omega = 3.4$ rps). Flow is left to right.

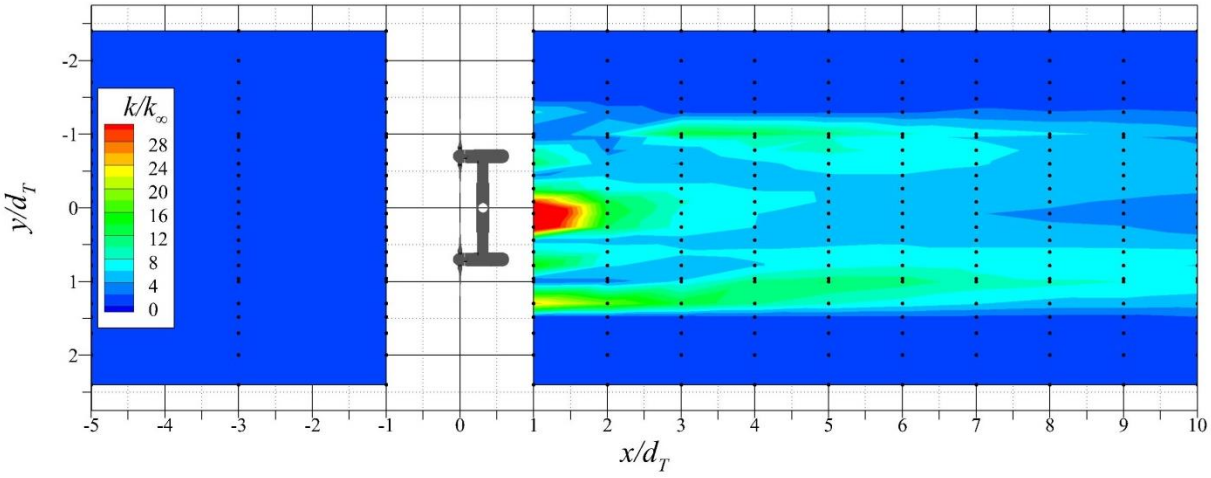

Figure 9: Normalized turbulent kinetic energy horizontal plane (XY) contours downstream of RM1 in the SAFL Main Channel. Turbine location indicated by the two circles at $x/d_T = 0$. Vertical axis, y/h_T, shows full SAFL Main Channel width (b = 2.75m). Black dots indicate actual ADV measurement locations. Measurements collected at $\lambda \approx 5.1$ (ω = 3.4 rps). Flow is left to right.

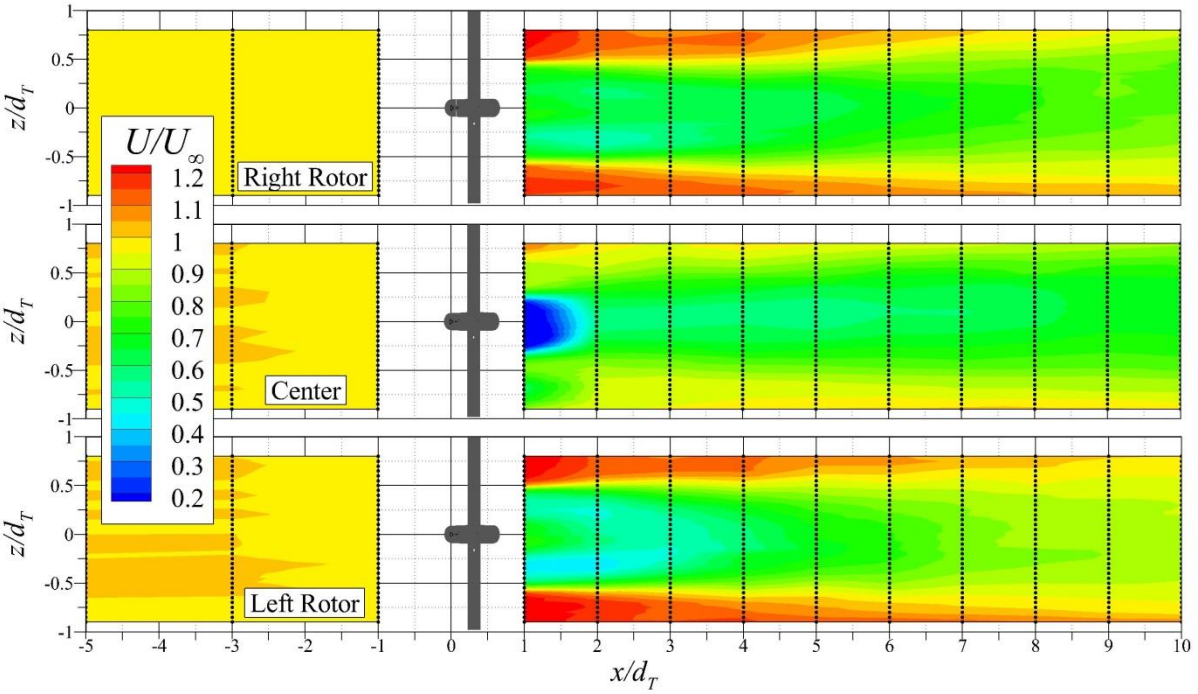

Figure 10: Normalized streamwise velocity vertical plane (XZ) contours upstream and downstream of RM1 in the SAFL Main Channel. Vertical axis, z/d_T, shows full water depth during the experiment (h = 1.0m). Vertical dotted black lines indicate actual ADV measurement profile locations. ADV vertical point spacing Δz = 0.025m (z/d_T = 0.05). Measurements collected at $\lambda \approx 5.1$ (ω = 3.4 rps). Flow is left to right.

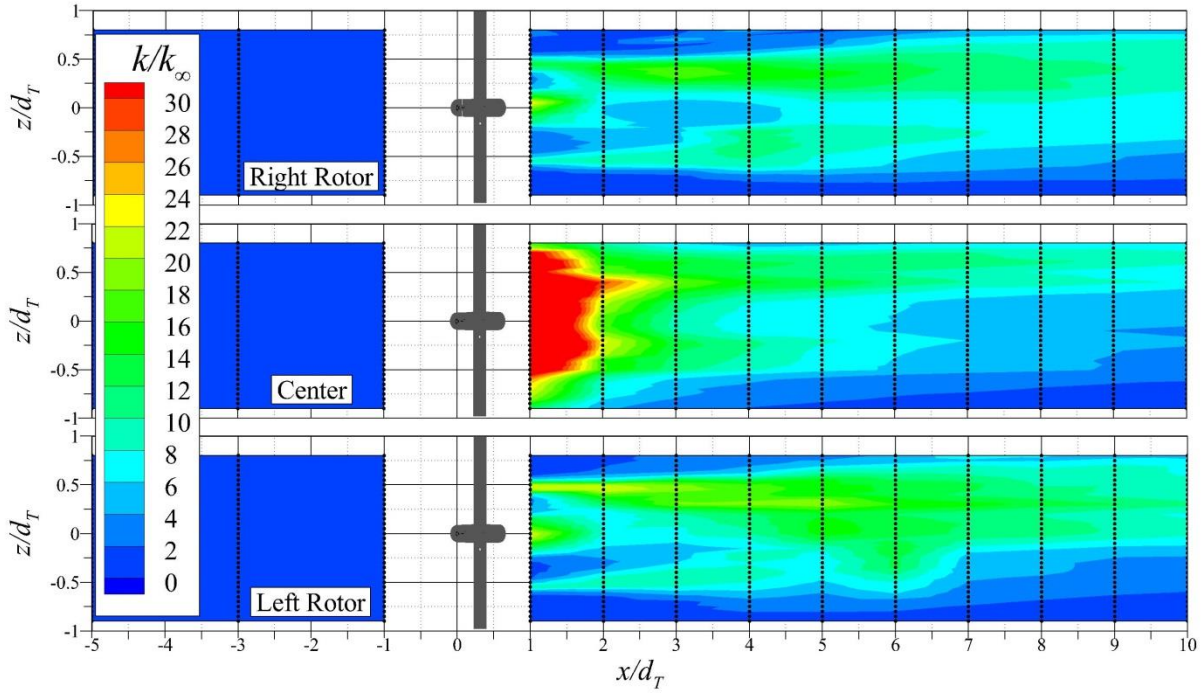

Figure 11: Normalized turbulent kinetic energy, k/k_∞, vertical plane (XZ) contours upstream and downstream of RM1 in the SAFL Main Channel. Vertical axis, z/d_T, shows full water depth during the experiment (h = 1.0m). Vertical dotted black lines indicate actual ADV measurement profile locations. ADV vertical point spacing Δz = 0.025m (z/d_T = 0.05). Measurements collected at $\lambda \approx 5.1$ (ω = 3.4 rps). Flow is left to right.

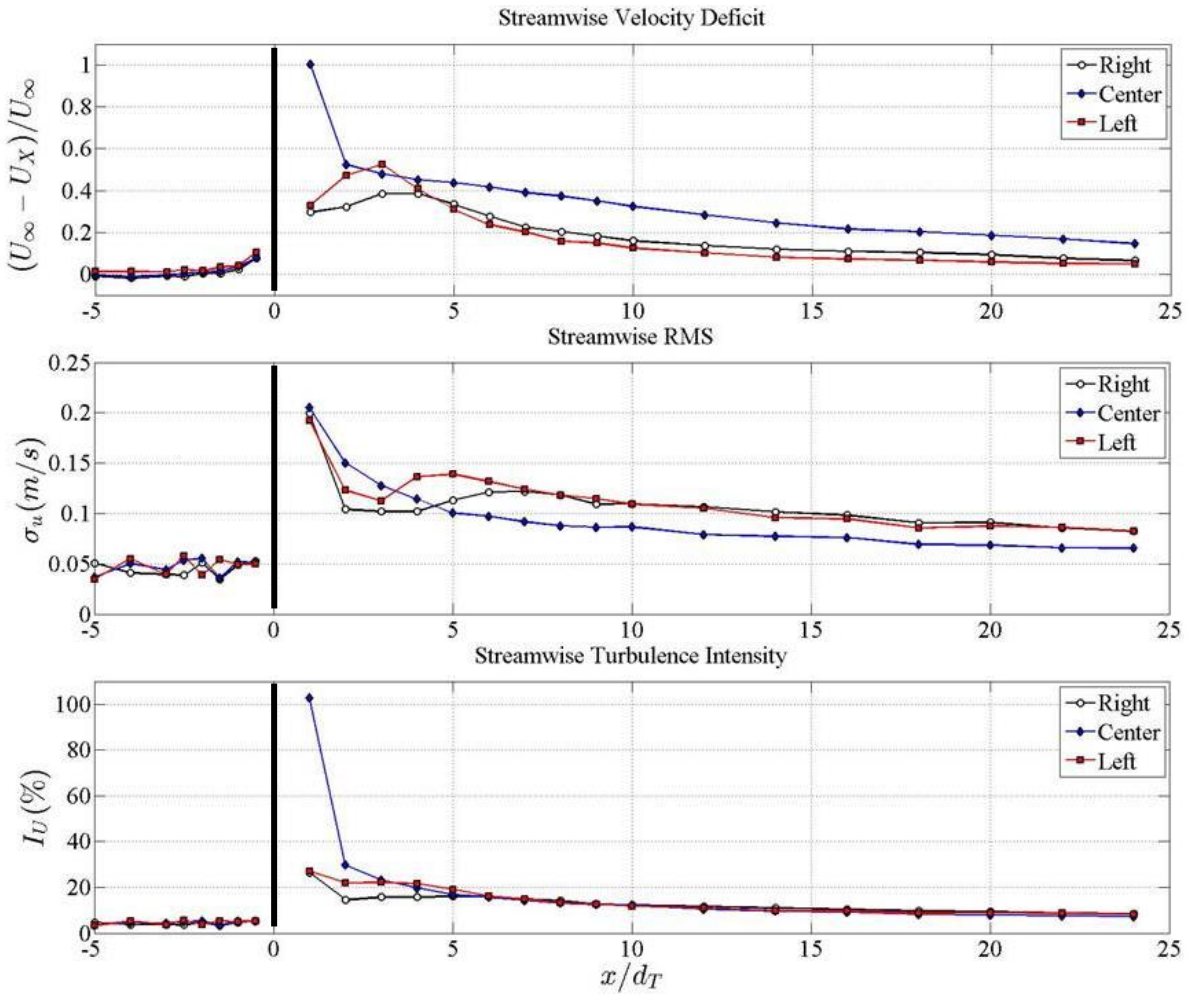

Figure 12: Rotor hub height velocity deficit (top); streamwise root-mean squared ($\sigma_U = \sqrt{\overline{u'^2}}$) (middle); and, streamwise turbulence intensity (bottom). RM1 rotors located at $x/d_T = 0$ (solid black vertical line). Measurements collected at $\lambda \approx 5.1$ ($\omega = 3.4$ rps). Flow is left to right.

V. Summary

The Reference Model 1 (RM1), a 1:40 geometrically scaled horizontal axis axial-flow hydrokinetic turbine designed by the U.S. DOE for tidal environments, was tested in the St. Anthony Falls Laboratory Main Channel facility at the University of Minnesota. Detailed performance and velocity measurements were collected to assess the interaction of RM1 with the surrounding environment. A robust dataset resulted from these experiments, providing exceptional data for model validation. Maximum C_P was found to occur near $\lambda \approx 5.1$ with values of $C_P = 0.48$ for the right rotor and $C_P = 0.43$ for the left rotor. Slight asymmetries in the approach flow environment may have caused the different turbine performance characteristics, but the root cause or causes were not determined. Detailed wake velocity measurements provide an indication of the turbulent wake environment, showing elevated levels of turbulent kinetic energy in the near wake environment, particularly resulting from the instabilities induced by the center support tower cylinder. Tip vortices also inject high turbulence levels that propagate up to approximately $4d_T$. Further investigations into the RM1 experimental data may reveal the mechanics of the near wake environment and the influence of von Karman frequencies shed from the center vertical and horizontal support arms have on the near wake structure of each rotor. What remains unknown is the effect of the

proximity of the rotor plane to the horizontal support arm downstream of each rotor and the cross arm effect on turbine performance. This structural feature likely does disrupt the near wake velocity and induce mixing more rapidly than other turbine configurations.

VI. Acknowledgment

This study was supported by the Department of Energy (DOE), Office of Energy Efficiency and Renewable Energy (EERE), Wind and Water Power Technologies Office (WWPTO). Sandia National Laboratories is a multi-program laboratory managed and operated by Sandia Corporation, a wholly owned subsidiary of Lockheed Martin Corporation, for the U.S. Department of Energy's National Nuclear Security Administration under contract DE-AC04-94AL85000.

VII. References

Chamorro, L.P., Hill, C., Morton, S., Ellis, C., Arndt, R.E.A., and Sotiropoulos, F. (2013). "On the interaction between a turbulent open channel flow and an axial-flow turbine." J. Fluid Mech., 716, 658-670.

Coleman, H.W., and Steele, W.G. (2009). *Experimentation, Validation, and Uncertainty Analysis for Engineers.* Third Edition, John Wiley & Sons, Inc. ISBN: 978-0-470-16888-2.

Goring, D.G. and Nikora, V.I., (2002), "Despiking acoustic Doppler velocimeter data," *J. Hydraulic Eng.*, 128(1), 117-126.

Gunawan, B., Neary, V.S., and McNutt, J., (2011), "ORNL ADV post-processing guide and MATLAB algorithms for MHK site flow and turbulence analysis," ORNL/TML-2011/338, September 2011, Prepared for the Wind and Water Power Program, Office of Energy Efficiency and Renewable Energy, U. S. Department of Energy, Washington, DC.

Lust, E.E., Luznik, L., Flack, K.A., Walker, J.M. and Van Bentham, M.C. (2013). "The influence of surface gravity waves on marine current turbine performance." *Int'l J. Marine Energy*, 3-4, 27-40.

Neary, V.S., Hill, C., Chamorro, L.P., Gunawan, B., and Sotiropoulos, F., (2012), "Experimental Test Plan – DOE Tidal and River Reference Turbines," ORNL/TM-2012/301, August 2012. Prepared for the Wind and Water Power Program, Office of Energy Efficiency and Renewable Energy, U. S. Department of Energy, Washington, DC.

Neary, V.S., Gunawan, B., Hill, C., and Chamorro, L.P., (2013), "Near and far field flow disturbances induced by model hydrokinetic turbine: ADV and ADP comparison," *Ren. Energy*, 60, 1-6.

Neary, V.S., Previsic, M., Jepsen, R.A., Lawson, M., Yu, Y., Copping, A.E., Fontaine, A.A., Hallett, K.C., and Murray, D.K., (2014a), "Methodology for design and economic analysis of Marine Energy Conversion (MEC) technologies." SAND-2014-9040, Sandia National Laboratories, 261 pages.

Neary, V.S., Lawson, M., Previsic, M., Copping, A., Hallett, K.C., LaBonte, A., Rieks, J., Murray, D., (2014b), "Methodology for design and economic analysis of marine energy conversion (MEC) technologies," Marine Energy Technology Symposium 2014 (METS2014), Seattle, WA, April 15-17.

VII. Appendix A: Tabulated summary of performance testing for RM1.

	Turbine variables						Performance		Inflow characteristics													
	RPM	**TSR (λ)**	**τ**	**F_t**	**P_t**	**R_c**	**C_t**	**C_p**	**U**	**V**	**W**	**σ_u**	**σ_v**	**σ_w**	**P_a**	**I_U**	**uu**	**vv**	**ww**	**uv**	**vw**	**uw**	**TKE**
	RPM	-	N-m	N	N-m/s	-	-	-	m/s	m/s	m/s	m/s	m/s	m/s	N-m/s	%	m^2/s^2	m^2/s^2	m^2/s^2	m^2/s^2	m^2/s^2	m^2/s^2	m^2/s^2
Right Rotor	60	1.51	0.682	n/a	4.299	9.08E+04	n/a	0.038	1.050	-0.010	0.008	0.043	0.047	0.034	114.026	4.05%	0.0018	0.0022	0.0011	0.0020	0.0016	0.0014	0.0026
	90	2.27	1.240	n/a	11.675	1.36E+05	n/a	0.105	1.048	-0.011	0.006	0.050	0.050	0.034	113.491	4.79%	0.0025	0.0025	0.0012	0.0025	0.0017	0.0017	0.0031
	120	3.02	2.847	n/a	35.770	1.82E+05	n/a	0.320	1.050	-0.011	0.003	0.051	0.048	0.035	114.222	4.89%	0.0026	0.0023	0.0012	0.0025	0.0017	0.0018	0.0031
	150	3.79	2.866	n/a	45.024	2.27E+05	n/a	0.408	1.045	-0.010	0.005	0.051	0.048	0.036	112.628	4.92%	0.0026	0.0023	0.0013	0.0025	0.0017	0.0018	0.0031
	168	4.26	2.813	n/a	49.487	2.55E+05	n/a	0.452	1.042	-0.012	0.003	0.051	0.048	0.034	111.627	4.89%	0.0026	0.0023	0.0012	0.0025	0.0016	0.0017	0.0030
	180	4.57	2.688	n/a	50.675	2.73E+05	n/a	0.467	1.039	-0.008	0.003	0.051	0.046	0.034	110.689	4.87%	0.0026	0.0021	0.0012	0.0023	0.0016	0.0017	0.0029
	192	4.87	2.558	n/a	51.429	2.90E+05	n/a	0.477	1.037	-0.009	0.004	0.052	0.048	0.034	110.058	5.04%	0.0027	0.0023	0.0012	0.0025	0.0017	0.0018	0.0031
	204	5.07	2.603	n/a	55.618	3.03E+05	n/a	0.476	1.042	-0.011	0.002	0.054	0.051	0.037	111.711	5.16%	0.0029	0.0026	0.0013	0.0028	0.0019	0.0020	0.0034
	216	5.45	2.298	n/a	51.990	3.28E+05	n/a	0.467	1.048	-0.010	0.000	0.051	0.047	0.034	113.437	4.86%	0.0026	0.0022	0.0012	0.0024	0.0016	0.0018	0.0030
	228	5.76	2.140	n/a	51.104	3.44E+05	n/a	0.471	1.040	-0.012	0.000	0.053	0.049	0.034	110.948	5.11%	0.0028	0.0024	0.0012	0.0026	0.0017	0.0018	0.0032
	240	6.07	1.964	n/a	49.368	3.62E+05	n/a	0.454	1.041	-0.010	-0.003	0.055	0.049	0.035	111.363	5.25%	0.0030	0.0024	0.0012	0.0027	0.0017	0.0019	0.0033
	252	6.35	1.832	n/a	48.369	3.81E+05	n/a	0.436	1.045	-0.010	-0.003	0.037	0.047	0.033	112.079	3.53%	0.0014	0.0022	0.0011	0.0017	0.0016	0.0012	0.0023
	270	6.82	1.611	n/a	45.557	4.09E+05	n/a	0.414	1.044	-0.012	-0.008	0.050	0.046	0.033	112.218	4.78%	0.0025	0.0021	0.0011	0.0023	0.0015	0.0016	0.0028
	300	7.57	1.290	n/a	40.525	4.54E+05	n/a	0.368	1.044	-0.011	-0.007	0.052	0.044	0.033	112.463	5.00%	0.0027	0.0020	0.0011	0.0023	0.0015	0.0017	0.0029
	330	8.32	0.939	n/a	32.472	4.98E+05	n/a	0.295	1.044	-0.011	-0.007	0.049	0.046	0.033	112.112	4.71%	0.0024	0.0021	0.0011	0.0023	0.0015	0.0016	0.0028
	360	9.05	0.675	n/a	25.473	5.44E+05	n/a	0.230	1.046	-0.011	-0.008	0.048	0.034	0.032	112.825	4.55%	0.0023	0.0012	0.0010	0.0016	0.0011	0.0015	0.0022
Left Rotor	60	1.51	0.639	n/a	4.025	9.02E+04	n/a	0.037	1.044	-0.006	0.010	0.056	0.049	0.035	112.360	5.35%	0.0031	0.0024	0.0013	0.0027	0.0017	0.0020	0.0034
	90	2.27	1.161	n/a	10.918	1.35E+05	n/a	0.102	1.036	-0.004	0.010	0.056	0.052	0.036	109.812	5.45%	0.0032	0.0027	0.0013	0.0029	0.0018	0.0020	0.0036
	120	3.02	2.515	n/a	31.605	1.80E+05	n/a	0.296	1.036	-0.004	0.014	0.059	0.052	0.038	109.901	5.67%	0.0035	0.0027	0.0014	0.0030	0.0020	0.0022	0.0038
	150	3.79	2.579	n/a	40.504	2.25E+05	n/a	0.379	1.036	-0.004	0.010	0.059	0.051	0.037	109.899	5.72%	0.0035	0.0026	0.0014	0.0030	0.0019	0.0022	0.0038
	168	4.26	2.404	n/a	42.291	2.52E+05	n/a	0.400	1.032	-0.005	0.012	0.059	0.051	0.036	108.698	5.73%	0.0035	0.0026	0.0013	0.0030	0.0018	0.0021	0.0037
	180	4.57	2.314	n/a	43.616	2.71E+05	n/a	0.412	1.032	-0.005	0.010	0.059	0.052	0.036	108.755	5.67%	0.0034	0.0027	0.0013	0.0030	0.0019	0.0021	0.0037
	192	4.87	2.160	n/a	43.444	2.89E+05	n/a	0.406	1.036	-0.005	0.009	0.057	0.051	0.037	109.841	5.52%	0.0033	0.0026	0.0013	0.0029	0.0019	0.0021	0.0036
	204	5.15	2.081	n/a	44.447	3.07E+05	n/a	0.412	1.039	-0.004	0.008	0.060	0.054	0.038	111.011	5.79%	0.0036	0.0029	0.0014	0.0032	0.0020	0.0023	0.0040
	216	5.45	1.920	n/a	43.430	3.24E+05	n/a	0.408	1.034	-0.004	0.007	0.057	0.049	0.036	109.171	5.49%	0.0032	0.0024	0.0013	0.0028	0.0018	0.0020	0.0035
	228	5.76	1.782	n/a	42.550	3.43E+05	n/a	0.394	1.038	-0.004	0.007	0.057	0.049	0.035	110.525	5.49%	0.0033	0.0024	0.0012	0.0028	0.0017	0.0020	0.0034
	240	6.07	1.676	n/a	42.114	3.61E+05	n/a	0.393	1.036	-0.005	0.008	0.058	0.048	0.035	110.045	5.58%	0.0033	0.0023	0.0013	0.0028	0.0017	0.0020	0.0035
	252	6.35	1.533	n/a	40.449	3.79E+05	n/a	0.372	1.040	-0.004	0.006	0.055	0.048	0.034	111.243	5.26%	0.0030	0.0023	0.0012	0.0026	0.0016	0.0019	0.0032
	270	6.82	1.227	n/a	34.694	4.06E+05	n/a	0.322	1.037	-0.002	0.004	0.053	0.047	0.033	110.013	5.08%	0.0028	0.0022	0.0011	0.0025	0.0015	0.0017	0.0030
	300	7.57	1.027	n/a	32.290	4.50E+05	n/a	0.302	1.035	-0.003	0.005	0.056	0.047	0.033	109.438	5.41%	0.0031	0.0022	0.0011	0.0026	0.0016	0.0019	0.0032
	330	8.32	0.650	n/a	22.474	4.96E+05	n/a	0.207	1.039	-0.005	0.001	0.054	0.046	0.033	110.730	5.20%	0.0029	0.0021	0.0011	0.0025	0.0015	0.0018	0.0031
	360	9.05	0.332	n/a	12.549	5.41E+05	n/a	0.115	1.041	-0.005	0.001	0.052	0.045	0.032	111.304	4.99%	0.0027	0.0020	0.0010	0.0023	0.0014	0.0016	0.0029

VIII. Appendix B: Inflow characteristics for $3d_T$ upstream of RM1.

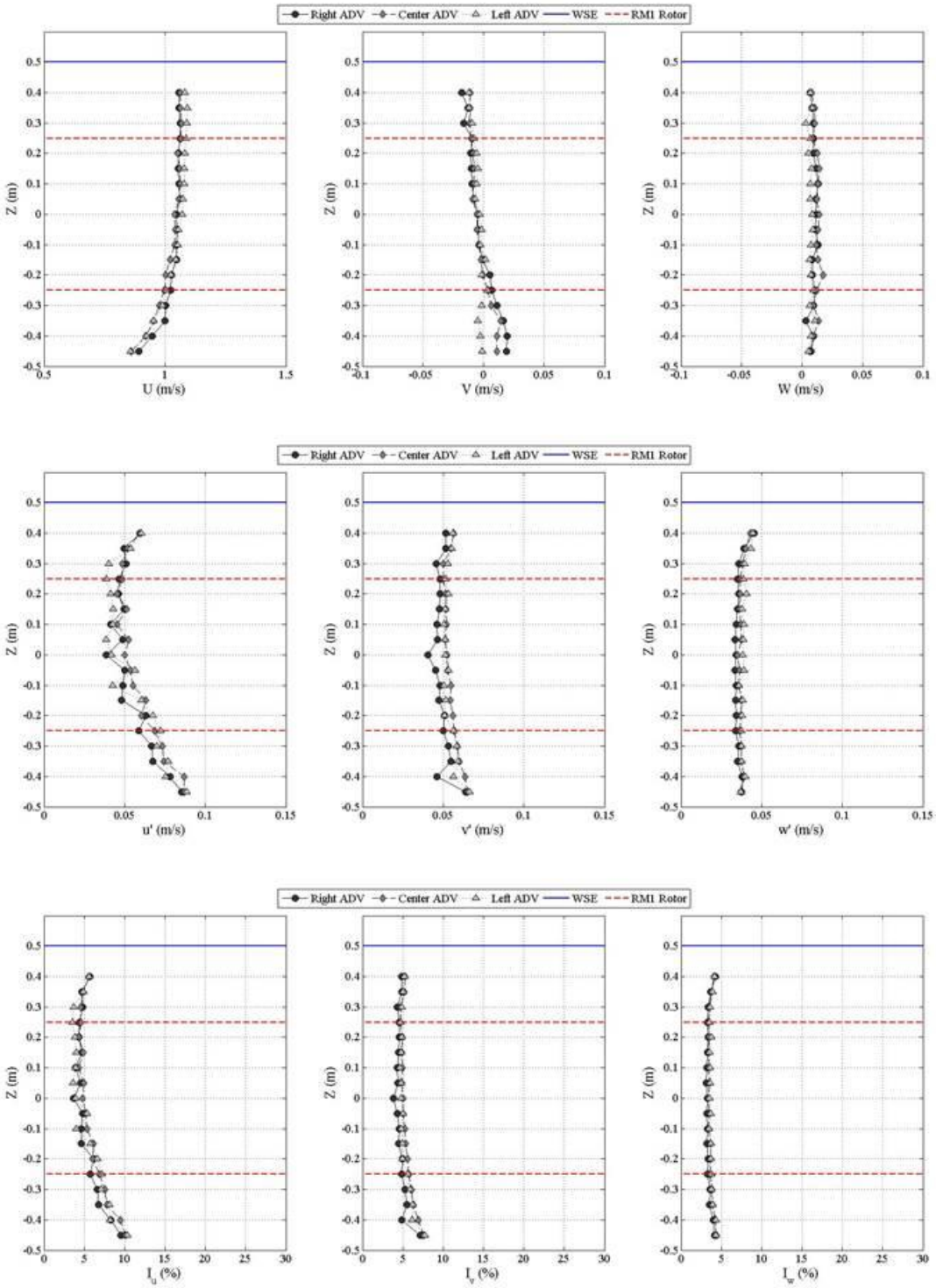

IX. Appendix C: Inflow characteristics for $5d_T$ upstream of RM1.